EDGE ARTICLE

Check for updates

Ligand-field transition-induced C–S bond formation from nickelacycles†

Jeongcheol Shin, ‡ Jiseon Lee, ‡ Jong-Min Suh and Kiyoung Park *

Photoexcitation is one of the acknowledged methods to activate Ni-based cross-coupling reactions, but factors that govern the photoactivity of organonickel complexes have not yet been established. Here we report the excited-state cross-coupling activities of Ni(II) metallacycle compounds, which display $\sim 10^4$ times enhancement for the C–S bond-forming reductive elimination reaction upon Ni-centered ligand-field transitions. The effects of excitation energy and ancillary ligands on photoactivity have been investigated with 17 different nickelacycle species in combination with four corresponding acyclic complexes. Spectroscopic and computational electronic structural characterizations reveal that, regardless of coordinated species, d–d transitions can induce Ni–C bond homolysis, and that the reactivity of the resulting Ni(I) species determines the products of the overall reaction. The photoactivity mechanism established in this study provides general insights into the excited-state chemistry of organonickel(II) complexes.

Introduction

Ni catalysts for cross-coupling reactions are economical and environment-friendly and show complementary reactivities to traditional Pd catalysts.[1] However, in conventional Ni-catalyzed cross-coupling reactions such as Negishi, Suzuki, and Kumada reactions, bond-forming reductive elimination (RE) reactions from the Ni(II) state involve endergonic thermodynamics and thus exhibit slow kinetics.[2] To promote this process, several strategies have been practiced. The chemical[3] or photochemical[2c,4] oxidation of the Ni(II) species to the high-valent states can increase the RE activity. Alternatively, electronic excitation of the Ni(II) species by energy transfer from photocatalysts or direct light irradiation can facilitate the RE reactions. This approach has been successfully implemented for diverse cross-coupling catalyses that include the C–C,[5] C–N,[6] C–O,[6a,7] and C–S[6a] bond-forming RE reactions.

Despite the increasing examples of excited-state Ni chemistries, no consensus has been reached on mechanisms, the understanding of which, though, is necessary for developing highly tunable and efficient photoreactions. For photoexcited Ni-mediated C–O cross-coupling reactions between aryl halide and carboxylic acid,[7a] several mechanisms have been suggested.[8] The transient absorption spectroscopic (TAS) studies of catalytically-relevant Ni(II)(2,2′-bipyridine; bpy)(aryl)Cl and
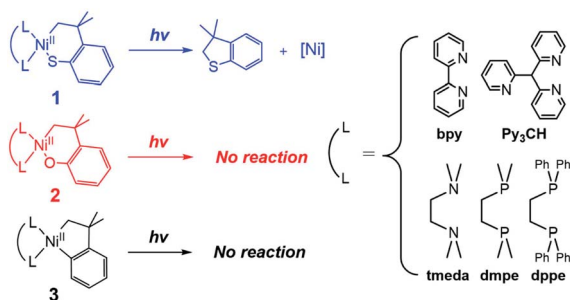
Ni(II)(bpy)(aryl)(acetate) complexes have revealed that Ni-to-bpy charge transfer (CT) transitions lead to a long-lived excited state (τ = 4 ns).[8a,c] In combination with transient infrared spectroscopy, Doyle *et al.* has defined this state to be a triplet d–d excited state, which is proposed to induce Ni–C bond homolysis in Ni(II)(bpy)(aryl)Cl on the basis of radical trapping experiment.[8b] Alternatively, MacMillan *et al.* has proposed that the long-lived state of Ni(II)(bpy)(aryl)(acetate) can induce the C–O bond-forming RE reaction directly.[8c] Regarding this system, Chen *et al.*'s multireference *ab initio* study has suggested that triplet Ni-to-bpy CT excited states, rather than d–d excited states, are the most viable excited states that can lead to the direct RE reaction.[8d] Meanwhile, Hadt *et al.*'s CASSCF study has provided new insights that a repulsive triplet carbon-to-Ni CT excited state can offer a spontaneous pathway for Ni–C bond homolysis.[8e]

In this study, the excited-state chemistry of three types of Ni(II) metallacycle compounds, with cycloneophyl ($-C_6H_4-o-C(CH_3)_2CH_2-$; CC hereinafter) and its oxa- ($-OC_6H_4-o-C(CH_3)_2CH_2-$; OC) and thia- ($-SC_6H_4-o-C(CH_3)_2CH_2-$; SC) derivative ligands (Scheme 1), have been investigated with five different ancillary ligands and seven different excitation energies. Nickelacycles and their heteroatom derivatives are key intermediates of various cyclization reactions between unsaturated compounds such as alkenes, alkynes, aldehydes, and imines.[1a,9] The C–C,[9b,10] C–N,[9d,11] C–O,[9c,12] and C–S[9e,13] bonds can be generated from Ni(II) metallacycle compounds, the RE reaction of which often limit catalytic turnover rates.[11f,14] Their excited-state reactivity has not been explored, while their electronic structural similarity to other Ni(II) complexes involved in photocatalysis suggests the possibility of light-induced

Department of Chemistry, Korea Advanced Institute of Science and Technology (KAIST), Daejeon 34141, Republic of Korea. E-mail: kiyoung.park@kaist.ac.kr

† Electronic supplementary information (ESI) available: Methods and materials, details of photoreactions, NMR, Abs, resonance Raman and MCD spectra of Ni complexes, and DFT-computed results. See DOI: 10.1039/d1sc05113j

‡ These authors contributed equally to this work.

Scheme 1 Excited-state RE reactions of nickelacycles.

reactions. To elucidate the electronic structures of the nickelacycles, electronic absorption (Abs), magnetic circular dichroism (MCD), and resonance Raman (rR) spectroscopies have been utilized in combination with density functional theory (DFT) computations. The effects of various excitation energies and ancillary ligands on photo-induced RE activity have been explored to specify RE-inducing excited states. The reaction coordinates of the excited-state RE reactions have also been established, providing insights into the factors that determine the RE activity of excited states.

Results and analysis

C–S bond-forming photoactivity as a function of excitation energy

Given that the bpy ligand had been proposed to play a major role in the photo-induced C–O coupling of the Ni^{II}(bpy)(aryl)(acetate) complex, bpy-bound nickelacycles, Ni^{II}(bpy)(SC) (**1**$_{bpy}$), Ni^{II}(bpy)(OC) (**2**$_{bpy}$), and Ni^{II}(bpy)(CC) (**3**$_{bpy}$), were first

Fig. 1 (a) 390 nm LED light-induced formation of RE products from **1**$_{bpy}$ (blue), **2**$_{bpy}$ (red), and **3**$_{bpy}$ (black), monitored by ^{1}H NMR spectroscopy. (b) Plots of the natural logarithm of the **1**$_{bpy}$ concentration *versus* irradiation time, obtained with the 325 (red), 355 (green), 405 (blue), 442 (purple), and 532 (black) nm laser lines with the normalized power of 50 mW. (c) Abs spectra of **1**$_{bpy}$ (top), **2**$_{bpy}$ (middle), and **3**$_{bpy}$ (bottom), overlaid with the 1st-order rate constants of the C–S coupling reaction and the C–O and C–C coupling yields obtained after 8 hours irradiation.

chosen for testing photoactivities (Fig. 1). These complexes are stable at 20 °C under dark conditions (Table S1†). Upon irradiation with 390 nm 52 W LED light, **1**$_{bpy}$ underwent quantitative C–S bond formation, yielding 99% conversion to 2,3-dihydro-3,3-dimethyl-benzo[b]thiophene within 3 hours (Fig. S1†). This photoactivity ($k_{390} \sim 3.6 \times 10^{-2}$ min^{-1}) indicates $\sim 10^4$ times acceleration for the RE reaction, compared to the dark reaction ($k_{dark} \sim 1.5$ (± 1.0) $\times 10^{-6}$ min^{-1} predicted for 20 °C by extrapolating Eyring plots from higher temperature data, Fig. S2†). The 390 nm LED-induced RE reaction follows the 1st-order kinetics, implying that the RE reaction is not induced by the generation of Ni^{III} complex *via* intermolecular electron transfer. Contrarily, no change was observed for **2**$_{bpy}$ and **3**$_{bpy}$ even after 1 day irradiation (Table S6†). This specific photoactivity of **1**$_{bpy}$ was unexpected, given the similarity in the Abs spectra of the three species (Fig. 1c).

To identify the excited states that lead to the C–S coupling reaction, seven different laser lines, 830, 633, 532, 442, 405, 355, and 325 nm, were examined. With the excitation energy higher than 500 nm, the 1st-order kinetics were observed with rate constants dependent on the laser power (Fig. 1b, S3 & S4†). Contrarily, with the excitation energy lower than 500 nm, the C–S coupling yield was negligible, although the Abs features maxed at 533 and 367 nm display comparable intensities (Fig. 1c & Table S2†). The fastest C–S bond formation was observed with the 405 nm excitation ($k_{405} = 4.2 \times 10^{-3}$ min^{-1}). This excitation-energy dependence implies that the photo-induced C–S coupling does not follow Kasha's rule.[15] Consistent with the 390 nm LED experiment, none of the laser lines could activate **2**$_{bpy}$ and **3**$_{bpy}$ despite the great similarity of their electronic structures (Fig. S5,† *vide infra*).

Electronic structure determination

The visible-range Abs and MCD spectra of **1**$_{bpy}$ are deconvoluted into five electronic transitions (Fig. 2). The Abs feature at 12 000–22 000 cm^{-1} with negligible RE activities contains bands 1 and 2, while bands 3–5 are associated with the RE-inducing Abs feature at 22 000–30 500 cm^{-1}. These five transitions display extinction coefficients of ~ 4000 M^{-1} cm^{-1},
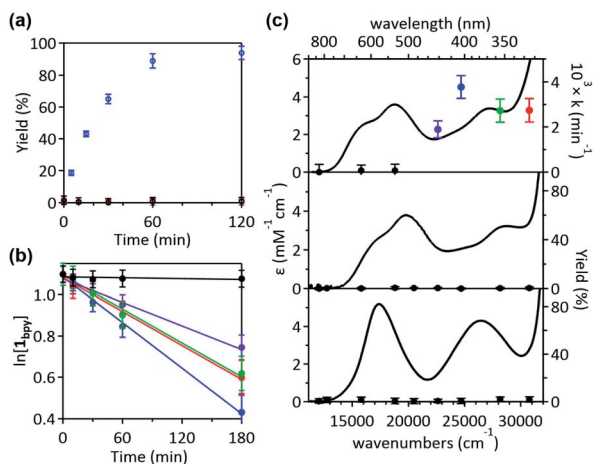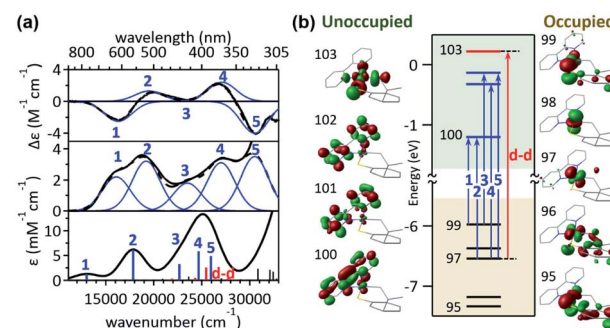

Fig. 2 (a) 5 T MCD (top), Abs (middle), and TDDFT-simulated Abs (bottom) spectra of **1**$_{bpy}$. The deconvoluted Gaussian bands and their sum spectra are shown in blue solid and black dashed lines, respectively. (b) MO diagram of **1**$_{bpy}$ and frontier MOs relevant to the electronic transitions in the visible region.

indicative of metal-to-ligand charge transfer (MLCT) transitions with $\varepsilon > 1000$ M^{-1} cm^{-1} rather than d–d transitions with $\varepsilon \sim 50$–500 M^{-1} cm^{-1}.[16] The rR spectra of 1_{bpy} support the Ni-to-bpy CT character, exhibiting enhanced intensities for bpy-based vibrations with laser excitation to bands 1 and 2 (Fig. S6 & S7†).[17]

This assignment is further confirmed by time-dependent density functional theory (TDDFT) computations, which were validated by the reproducibility of the $1_{bpy} \sim 3_{bpy}$ Abs spectra (Fig. S10†). The simulated spectrum obtained with the LC-ωPBE functional[18] ($\omega = 0.15$) and the 6-311g(d,p) basis set[19] shows that bands 1–5 can be associated with charge transfer transitions from the Ni $3d_{yz}$ and $3d_{xz}$-based molecular orbitals (MOs) to the bpy π^*-based MOs (Table S3†). This similar Ni-to-bpy CT character of the five bands contrasts with the distinct photoactivities of bands 3–5 relative to bands 1 and 2. To explain the differential photoactivities, transitions with even small oscillation strengths were thoroughly analyzed, revealing that Ni-centered d–d transitions contribute to the energy range of bands 3–5, but not that of bands 1 and 2. Notably, the Abs and MCD spectral features of 2_{bpy} and 3_{bpy} can also be attributed to Ni-to-bpy π^* CT transitions similarly to 1_{bpy}, based on the rR enhancement of bpy-based vibrations and TDDFT-simulated Abs spectra (Fig. S6–S9 and Tables S4, S5†).

Ancillary ligand variations to elucidate photoactive excited states

To unmask the ligand-field transitions from the MLCT-dominant Abs bands, the bpy ligand was replaced with other ancillary ligands. The less-conjugated pyridinyl ligand, tris(2-pyridinyl)methane (Py_3CH), was introduced with anticipation of upshifting the MLCT transitions in the spectrum, as the pyridinyl π^* system has higher energy than the bpy π^* system. However, at 390 nm, 1_{Py3CH} still displays a similar Abs intensity and the comparable photo-induced RE activity as 1_{bpy} (Fig. 3). With the 1,2-bis(diphenylphosphino)ethane (dppe) ligand, 1_{dppe} also displays unexpected Ni-to-dppe phenyl π^* transitions in the visible region. Detailed electronic spectral assignments are given in ESI (Fig. S14, S15, and Tables S7, S8†).

Alternatively, with the aliphatic amine ligand, N,N,N',N'-tetramethylethylenediamine (tmeda), which does not contain low-lying ligand-based unoccupied MOs, the Ni^{II}(tmeda)(SC) complex, 1_{tmeda}, exhibits a significantly reduced Abs intensity at the energy below 350 nm (Fig. 3a). Notably, 1_{tmeda} displays an almost identical photoactivity as 1_{bpy} ($k_{390} = 5.0 \times 10^{-2}$ min^{-1} for 1_{tmeda} and 3.6×10^{-2} min^{-1} for 1_{bpy}), despite the 13 times reduced absorptivity of 1_{tmeda} relative to 1_{bpy} ($\varepsilon_{390} = 213$ M^{-1} cm^{-1} for 1_{tmeda} and 2775 M^{-1} cm^{-1} for 1_{bpy}). With the aliphatic phosphine ligand, 1,2-bis(dimethylphosphino)ethane (dmpe), 1_{dmpe} also exhibits low-intensity Abs at 380–450 nm, and undergoes the RE reaction with the similar photoactivity as 1_{tmeda} (Fig. 3d).

To elucidate the low-intensity Abs features in the visible range of 1_{tmeda}, its Abs and MCD spectra were deconvoluted and compared to the TDDFT-calculated electronic transitions (Fig. 4). With the aliphatic ancillary ligand, the frontier MOs (FMOs) of 1_{tmeda} are all Ni 3d-based, and thus only the d–d transitions
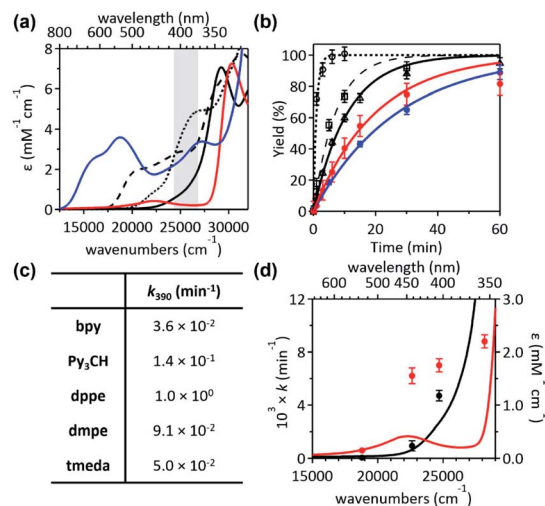

Fig. 3 (a) Abs spectra and (b) ^{1}H-NMR monitored C–S coupled product formation as a function of 390 nm LED irradiation time of 1_{bpy} (blue solid, •), 1_{Py3CH} (black dashed, □), 1_{dppe} (black dotted, ○), 1_{dmpe} (black solid, △), and 1_{tmeda} (red solid, •). The energy window of light emitted from the 390 nm LED lamp is highlighted in gray. (c) 390 nm LED-induced RE rate constants. (d) Excitation energy-dependent C–S coupling rate constants of 1_{tmeda} (red) and 1_{dmpe} (black), overlaid with their Abs spectra. Detailed kinetic analyses are given in Fig. S11–S13 and Table S6.†

contribute to the visible energy region (Table S9†). The spectra of 1_{dmpe} could also be assigned similarly (Fig. S16 and Table S10†). These electronic structural characterizations reveal that the ligand-field transitions alone can drive the C–S bond-forming RE reaction. Depending on the ancillary ligands, Abs intensities may vary due to contributions from the MLCT transitions. However, the photoactivities of the five **1** complexes are still comparable, as the d–d excited states of the five species are similarly effective for the RE reaction. The results above do not exclude the possibility of high-energy MLCT transitions, such as those in bands 3–5 of 1_{bpy}, being effective in inducing the RE reaction. Nevertheless, the roles of the ancillary ligands appear to be minor, as d–d transitions suffice for performing the photoreactions of **1**'s.
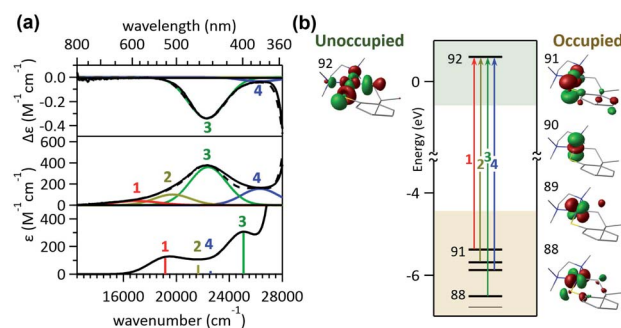

Fig. 4 (a) 5 T MCD (top), Abs (middle), and TDDFT-simulated Abs (bottom) spectra of 1_{tmeda}. The deconvoluted Gaussian bands and their sum spectra are shown in colored solid and black dashed lines, respectively. (b) MO diagram of 1_{tmeda} and frontier MOs relevant to the electronic transitions in the visible region.

It should also be noted that, regardless of the ancillary ligands, complexes **2** and **3** remain photo-inactive, although their Abs and MCD spectra are essentially identical to those of corresponding complexes **1** (Fig. S17–S20†). These distinctive photoactivities despite the similar electronic structures imply that the RE-inducing photoactivity would not be solely determined by the initial excited states at the reactant state. Thus, to explore variations in the excited states along the RE reaction coordinate, the excited-state potential energy surfaces (PESs) of **1$_{tmeda}$**, **2$_{tmeda}$**, and **3$_{tmeda}$** have been plotted by performing TDDFT computations on the ground-state PESs (Fig. 5a & S26†).

Excited-state potential energy surfaces

To search for the reaction coordinate of the C–S bond-forming RE reaction, the PES of **1$_{tmeda}$** has been plotted along the Ni–C and C–S bond lengths. At the ground state, the RE reaction from the Ni^{II}(SC^{2-}) reactant (**R**, red PES in Fig. 5a) to the Ni^0 + SC^0 product (**P**, blue PES in Fig. 5a) involves one elementary step with two electrons transferred from the SC ligand to the Ni^{II} center. This step is endergonic (ΔG; ΔH; ΔE ~18, 18, 19 kcal mol^{-1}) with a high kinetic barrier of $\Delta G^{\ddagger}$; $\Delta H^{\ddagger}$; $\Delta E^{\ddagger}$ ~39, 39, 41 kcal mol^{-1}, consistent with the poor RE activity under dark conditions (Fig. S23†). Alternatively, at the T$_1$ state (cyan PES in Fig. 5a), which is accessible via intersystem crossing (ISC) following photoexcitation, the RE reaction should involve two one-electron transfer steps, as the T$_1$ state contains two singly occupied MOs with the electronic configuration of $(d_{z^2})^1(d_{x^2-y^2})^1$ (Fig. S24†). The 1st electron transfer occurs from the C-based HOMO to the Ni 3d$_{z^2}$-based spin-down LUMO, leading to the Ni–C bond homolysis and forming the Ni^I(SC$^{\bullet-}$) intermediate (**I**, black PES in Fig. 5a). **I** contains two radical sites at the Ni^I center and the C moiety apart by ~3.5 Å, far enough to render the singlet and triplet states degenerate. Subsequently, to form the C–S bond in a spin-allowed fashion, the 2nd electron

transfer should occur to the Ni 4s-based MO for triplet **I**, while for singlet **I**, the lower-energy Ni 3d$_{x^2-y^2}$-based MO can be an acceptor. Thus, the former process involves less favorable thermodynamics than the latter one, indicating that the triplet intermediate generated from photoexcitation should undergo ISC prior to the C–S bond formation (Fig. S25†).

To form intermediate **I** from the ligand-field excited states, TDDFT-calculated PESs propose two plausible pathways, one via ^{1}(dd) → T$_1$ ISC and the other via ^{1}(dd) → ^{3}(C-to-Ni CT) ISC (red dashed vs. solid pathways in Fig. 5a). The former pathway is parallel to the previously suggested mechanism based on the TAS study of Ni^{II}(bpy)(aryl)Cl.[8b] This process is calculated to be uphill by $\Delta G^{\ddagger}$ ~ 22.5 kcal mol^{-1} for **1$_{tmeda}$** (cyan PES → black PES in Fig. 5a) and 26.0 for **1$_{bpy}$** (Table S13†). Hadt et al. has shown that DFT calculations tend to underestimate the corresponding barrier.[8e] Moreover, the excitation energy dependence of the photoreaction of **1$_{bpy}$** proposes that the T$_1$-to-intermediate **I** conversion is unlikely. Alternatively, in the vicinity of the ^{1}(dd) state (green PES in Fig. 5a), a repulsive PES is calculated, associated with the triplet C ligand-to-Ni CT transition (yellow PES in Fig. 5a). From the ^{1}(dd) state, this ^{3}(C-to-Ni CT) state can be accessed with a minor elongation of the Ni–C bond by ~0.1 Å and a small barrier of ~5 kcal mol^{-1}. Since the ^{3}(C-to-Ni CT) state is equivalent to intermediate **I** in terms of the Ni^I(SC$^{\bullet-}$) electronic configuration (Fig. 5b), once ISC from the ^{1}(dd) state to the ^{3}(C-to-Ni CT) state occurs, the formation of **I** and subsequently **P** can proceed in a downhill fashion with no major barriers (red solid path in Fig. 5a). The presence of a similar repulsive PES was predicted in the previous multireference computational study of the Ni^{II}(bpy)(Ar) complexes, for which, though, the Ni-to-bpy CT excited state was proposed to be the initial state.[8e] From the Ni–C bond dissociated intermediate **I**, **R** and **P** are equally accessible with no discernible barriers. This explains a small
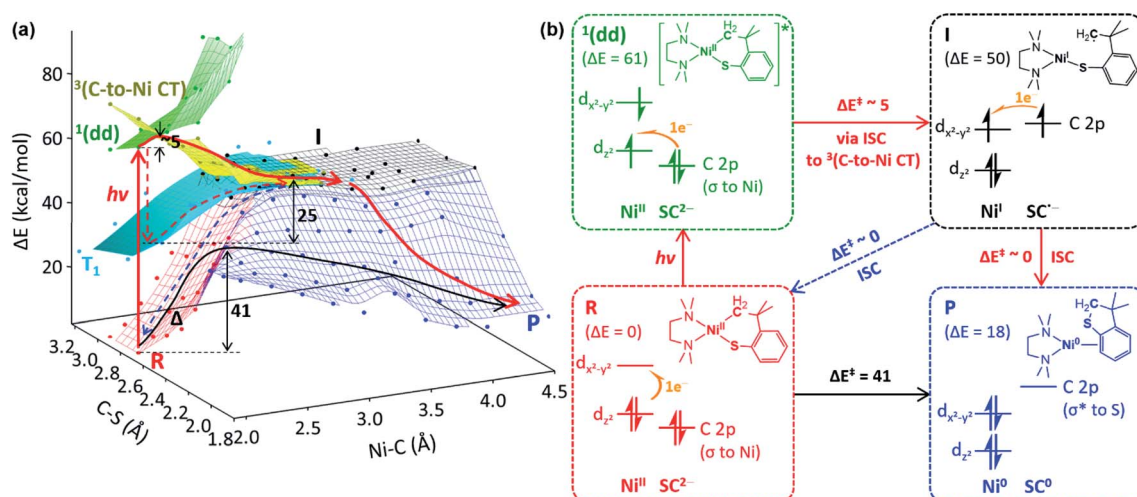

Fig. 5 (a) The ground- and excited-state PESs of **1$_{tmeda}$**, colored according to the electronic configurations of the ground state (red) and the ^{1}(dd) (green), ^{3}(C-to-Ni CT) (yellow), and T$_1$ (cyan) excited states of the Ni^{II}(SC^{2-}) reactant (**R**, red), the Ni^I(SC$^{\bullet-}$) intermediate (**I**, black), and the Ni^0 + SC^0 product (**P**, blue). A plausible photo-induced RE pathway from the ^{1}(dd) state and the dark RE pathway are drawn with red and black solid arrows, respectively. Alternative paths are noted with dashed arrows. (b) Electronic configuration and potential energy (in kcal mol^{-1}) changes over the reactions presented in (a).

quantum yield of 6.8×10^{-3} estimated relative to ferrioxalate actinometry (Fig. S27†).

Ni–C bond homolysis induced by ligand-field excitations

To confirm the presence of intermediate **I** for **1**, radical trapping experiments with α-phenyl-*N*-tertiary-butylnitrone (PBN) and (2,2,6,6-tetramethylpiperidin-1-yl)oxyl (TEMPO) were attempted but unsuccessful. Nevertheless, this result is understandable, because the subsequent reactions of intermediate **I** are predicted to have no barriers. Another factor that would limit the lifetime of intermediate **I** is the chelate effect of the SC ligand, which assists the intramolecular reaction of the carbon radical. Thus, an analogous acyclic complex, $Ni^{II}(bpy)(Me)(SPh)$ (**4**$_{bpy}$), has been explored. The Abs and MCD spectra of **4**$_{bpy}$ are essentially identical to those of **1**$_{bpy}$, as the same type of electronic transitions, Ni-to-bpy CT and d–d transitions, contribute to the spectra (Fig. 6b & S28†). Upon 390 nm LED irradiation, unlike **1**$_{bpy}$ that forms the C–S coupled product homogeneously, **4**$_{bpy}$ yields ethane majorly (Fig. 6a). These products indicate the photo-induced generation of methyl radicals; *i.e.*, the photoexcitation of **4**$_{bpy}$ affects the Ni–C bond homolysis, which could be further confirmed by the radical-trap EPR signal (Fig. S29†). For both **1**$_{bpy}$ and **4**$_{bpy}$, the repulsive ^{3}(C-to-Ni CT) PES's are calculated, suggesting that the Ni–C bond homolysis can be photo-induced for both complexes (Fig. S31†). Subsequent to this step, while **1**$_{bpy}$ can undergo the intramolecular C–S bond formation with a minor barrier, the dissociated methyl radical of **4**$_{bpy}$ kinetically and thermodynamically prefers the ethane formation to the C–S coupled thioanisole generation (Fig. S32†).

The excitation-energy-dependent photoactivity of **4**$_{bpy}$ is also equivalent to that of **1**$_{bpy}$, supporting that, regardless of

whether the system is cyclic or acyclic, the photo-induced initial step is identical. Fig. 1 shows that **1**$_{bpy}$ decays rapidly with excitation to bands 3–5, while excitation to bands 1–2 displays negligible effects. Likewise, a faster decay of **4**$_{bpy}$ was observed with the 405 nm irradiation aiming band 3 than with the 532 nm irradiation associated with band 2 (Fig. S30†). Similar rate-constant ratios, k_{405}/k_{532}, were obtained for **1**$_{bpy}$ (40) and **4**$_{bpy}$ (34), indicating the equivalence of the photo-induced step (Fig. 6c). The excitation energy dependence of the Ni–C bond homolysis supports the significance of the dissociative ^{3}(C-to-Ni CT) PES, which is more accessible from the higher-energy d–d excited states than the lower-energy Ni-to-bpy CT states. The effectiveness of ligand-field excitations on the Ni–C bond homolysis was further confirmed with $Ni^{II}(dmpe)(Me)(SPh)$ (**4**$_{dmpe}$), which has only d–d transitions in the visible region and exhibits a comparable photoactivity ($k_{405} \sim 3.7 \times 10^{-2}$ min^{-1}, Fig. S33†).

Ni^I intermediates determine the overall photo-reactivity

The above mechanistic studies of **1** and **4** indicate that during the photo-induced Ni–C bond homolysis, the sulfur moiety of the SC ligand does not play a specific role. This finding leaves a question of why **2** and **3** are photo-inactive despite the similar electronic structures. To test whether the Ni–C bond homolysis can still be induced in the absence of the sulfenyl group, the photo-reactivities of $Ni^{II}(dmpe)(Me)(OPh)$ (**5**$_{dmpe}$) and $Ni^{II}(dmpe)Me_2$ (**6**$_{dmpe}$) have been compared to **4**$_{dmpe}$. Upon 390 nm LED irradiation which can induce d–d transitions (Fig. S34†), all three complexes produce a sizable amount of ethane (Fig. 7a). This result reveals that the Ni–C bond homolysis can be photo-induced regardless of the ligands, being not unique to the sulfur-ligated systems. This conclusion is further supported by aliphatic nickelacycles, $Ni^{II}(bpy)(CH_2CH_2CH_2\text{-}CH_2)$ (**7**$_{bpy}$) and $Ni^{II}(bpy)(OCH_2CH_2CH_2CH_2)$ (**8**$_{bpy}$). Under 390 nm irradiation, these systems generate β-hydride elimination products, indicating that the Ni–C bond homolysis can be photo-induced regardless of cyclic or acyclic compounds (Table S15†). These results imply that **2** and **3** could also undergo the photo-induced Ni–C bond homolysis. Consistently, the TDDFT-calculated excited state PESs of **2** and **3** with the tmeda and dmpe ligands predict the presence of the repulsive ^{3}(C-to-Ni CT) states nearby the ^{1}(dd) states (Fig. S26 & S35†).

The fact that only **1** generates the RE product while all **1–3** can undergo the Ni–C bond homolysis upon ligand-field excitations proposes that the reactivities of the Ni^I intermediates can be variable depending on the substrate. In Fig. 5a, the PESs of **1**$_{tmeda}$ show that intermediate **I** can undergo either the C–S bond formation that produces the RE product or the Ni–C radical recombination that leads back to the reactant. The similar pathways are also calculated for **1**$_{dmpe}$ ∼ **3**$_{dmpe}$ (Fig. S36–S38†). The C–S bond formation from the Ni^I intermediate of **1**$_{dmpe}$ is almost barrierless (Fig. 7b). However, for **2**$_{dmpe}$ and **3**$_{dmpe}$, the C–C and C–O bond formations from the Ni^I intermediates involve 7–11 kcal mol^{-1} higher kinetic barriers than the Ni–C radical recombination. Therefore, overall only **1**$_{dmpe}$ displays the photo-induced RE activity, while **2**$_{dmpe}$ and **3**$_{dmpe}$
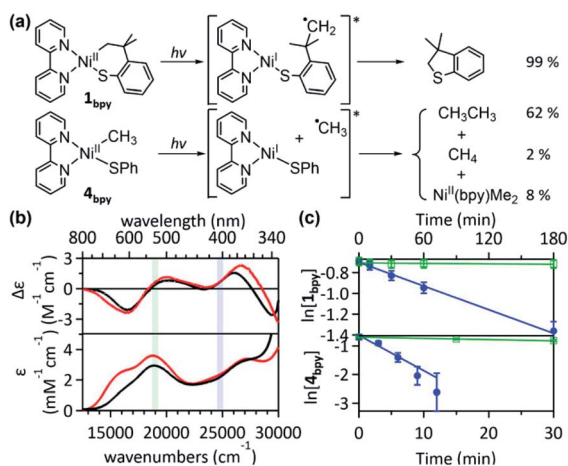

Fig. 6 (a) 390 nm LED-induced reactions of **1**$_{bpy}$ (top) and **4**$_{bpy}$ (bottom). For **4**$_{bpy}$, the yield is given per methyl group. (b) 5 T MCD (top) and Abs (bottom) spectra of **1**$_{bpy}$ (red) and **4**$_{bpy}$ (black), with the 405 nm (blue) and 532 nm (green) laser excitation energies shaded. (c) Logarithmic plots for the ^{1}H NMR-monitored decays of **1**$_{bpy}$ (top) and **4**$_{bpy}$ (bottom) as a function of 405 nm (blue) and 532 nm (green) laser irradiation time. The linear regression fitting gives $k_{532} = 2 \times 10^{-4}$ min^{-1} and $k_{405} = 4.2 \times 10^{-3}$ min^{-1} for **1**$_{bpy}$ and $k_{532} = 3.5 \times 10^{-3}$ min^{-1} and $k_{405} = 1.2 \times 10^{-1}$ min^{-1} for **4**$_{bpy}$.
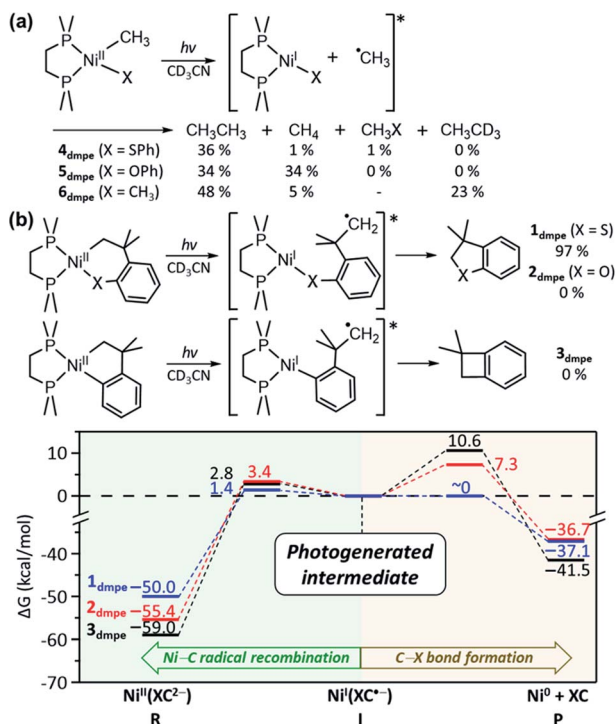
Fig. 7 (a) Photoreactions of 4_{dmpe}, 5_{dmpe}, and 6_{dmpe}. The final yields are given with respect to the initial concentrations of the methyl groups. (b) Energy profiles for the reactions of the Ni^I intermediates generated upon Ni–C bond homolysis of 1_{dmpe} (blue), 2_{dmpe} (red), and 3_{dmpe} (black).

are seemingly photo-inactive. The same tendency is calculated for $1_{tmeda} \sim 3_{tmeda}$ and 1_{bpy} (Fig. S39–S43†).

Discussions

We have shown that visible-light photoexcitation can enhance the C–S coupling activity of **1** by four orders of magnitude. To understand its mechanism, the effects of diverse ancillary ligands have been explored, along with electronic structural characterizations by Abs and MCD spectroscopies and TDDFT computations. These analyses reveal that, without bpy-associated transitions, d–d excitations alone can drive the C–S bond-forming RE reaction. The excitation-energy-dependent photoactivity of 1_{bpy} demonstrates that the photo-induced C–S bond formation does not follow Kasha's rule, emphasizing the significance of ISC to the dissociative ^{3}(C-to-Ni CT) state that leads to the Ni–C bond homolysis. This reactivity parallels the C–C coupling photo-activity of high-valent nickelacycles, which display the maximum RE rate upon C-to-Ni CT transitions.[20] This excitation-energy-dependent photochemistry is not unprecedented for transition metal complexes. The Cu–Cl bond homolysis of a chlorobis(phenanthroline)Cu^{II} complex can be induced by Cl-to-Cu CT transition (427 or 470 nm) but not by d–d transitions (785 or 800 nm).[21] $Mn_2(CO)_{10}$ undergoes the Mn–Mn bond homolysis with 350 nm light, while 248 and 193 nm light causes CO loss.[22] These examples emphasize the significance of electronic structure characterizations in utilizing excited-state chemistry.

The ligand-field transition-induced Ni–C bond homolysis is found to be general for organonickel(II) complexes **1–8**, regardless of ancillary ligands and neighboring coordinated species. However, the final product of the photoreactions can be variable, depending on the reactivities of the Ni^I intermediates and carbon radicals obtained from the photo-induced Ni–C bond homolysis. The DFT-computed reaction coordinates reveal that the Ni^I intermediates of **1** can undergo the barrier-less C–S bond formation, while those of **2–3**, acyclic compounds **4–6**, and aliphatic nickelacycles **7–8** prefer the recombination of the Ni–C bond, ethane formation, and β-hydride elimination, respectively. This mechanistic elucidation provides a general basis for understanding and designing the excited-state chemistry of organonickel(II) complexes, proposing that to control their photochemistry, the reactivity of intermediates resulting from Ni–C bond homolysis should be concerned. Considering the entropy-driven dissociation of organic radicals in acyclic compounds, this study suggests that nickelacycles can be a good platform for selective photochemistry as shown in the visible-light-induced C–S bond formation of **1**.

Data availability

The NMR, Abs, MCD, and rR spectra of Ni complexes and DFT-computation results including Cartesian coordinates can be found in ESI.†

Author contributions

J. Shin and J. Lee performed all syntheses, kinetic investigations, and spectroscopic and computational characterizations. J. Suh performed ESI-MS analyses. K. Park supervised research activities. All authors contributed to the final version of the manuscript.

Conflicts of interest

There are no conflicts to declare.

Acknowledgements

Notes and references

1 (a) S. Z. Tasker, E. A. Standley and T. F. Jamison, *Nature*, 2014, **509**, 299–309; (b) J. Twilton, C. Le, P. Zhang, M. H. Shaw, R. W. Evans and D. W. C. MacMillan, *Nat. Rev. Chem.*, 2017, **1**, 0052; (c) B. M. Rosen, K. W. Quasdorf, D. A. Wilson, N. Zhang, A. M. Resmerita, N. K. Garg and V. Percec, *Chem. Rev.*, 2011, **111**, 1346–1416; (d) V. B. Phapale and D. J. Cardenas, *Chem. Soc. Rev.*, 2009, **38**,

1598–1607; (e) F. S. Han, *Chem. Soc. Rev.*, 2013, **42**, 5270–5298.

2 (a) R. Y. Han and G. L. Hillhouse, *J. Am. Chem. Soc.*, 1997, **119**, 8135–8136; (b) S. A. Macgregor, G. W. Neave and C. Smith, *Faraday Discuss.*, 2003, **124**, 111–127; (c) J. A. Terrett, J. D. Cuthbertson, V. W. Shurtleff and D. W. C. MacMillan, *Nature*, 2015, **524**, 330–334; (d) M. Busch, M. D. Wodrich and C. Corminboeuf, *ACS Catal.*, 2017, **7**, 5643–5653; (e) P. M. MacQueen, J. P. Tassone, C. Diaz and M. Stradiotto, *J. Am. Chem. Soc.*, 2018, **140**, 5023–5027.

3 (a) K. M. Koo, G. L. Hillhouse and A. L. Rheingold, *Organometallics*, 1995, **14**, 456–460; (b) R. Han and G. L. Hillhouse, *J. Am. Chem. Soc.*, 1998, **120**, 7657–7658; (c) N. Nebra, *Molecules*, 2020, **25**, 2015; (d) F. L. Vaillant, E. J. Reijerse, M. Leutzsch and J. Cornella, *J. Am. Chem. Soc.*, 2020, **142**, 19540–19550.

4 (a) O. S. Wenger, *Chem.–Eur. J.*, 2021, **27**, 2270–2278; (b) Z. W. Zuo, D. T. Ahneman, L. L. Chu, J. A. Terrett, A. G. Doyle and D. W. C. MacMillan, *Science*, 2014, **345**, 437–440; (c) J. C. Tellis, D. N. Primer and G. A. Molander, *Science*, 2014, **345**, 433–436; (d) J. Xuan, T. T. Zeng, J. R. Chen, L. Q. Lu and W. J. Xiao, *Chem.–Eur. J.*, 2015, **21**, 4962–4965; (e) M. S. Oderinde, M. Frenette, D. W. Robbins, B. Aquila and J. W. Johannes, *J. Am. Chem. Soc.*, 2016, **138**, 1760–1763; (f) I. Abdiaj, A. Fontana, M. V. Gomez, A. de la Hoz and J. Alcázar, *Angew. Chem., Int. Ed.*, 2018, **57**, 8473–8477; (g) R. Sun, Y. Z. Qin and D. G. Nocera, *Angew. Chem., Int. Ed.*, 2020, **59**, 9527–9533.

5 (a) D. R. Heitz, J. C. Tellis and G. A. Molander, *J. Am. Chem. Soc.*, 2016, **138**, 12715–12718; (b) L. Huang and M. Rueping, *Angew. Chem., Int. Ed.*, 2018, **57**, 10333–10337; (c) D. L. Zhu, R. J. Xu, Q. Wu, H. Y. Li, J. P. Lang and H. X. Li, *J. Org. Chem.*, 2020, **85**, 9201–9212.

6 (a) R. A. Escobar and J. W. Johannes, *Chem.–Eur. J.*, 2020, **26**, 5168–5173; (b) C. H. Lim, M. Kudisch, B. Liu and G. M. Miyake, *J. Am. Chem. Soc.*, 2018, **140**, 7667–7673; (c) M. Kudisch, C. H. Lim, P. Thordarson and G. M. Miyake, *J. Am. Chem. Soc.*, 2019, **141**, 19479–19486; (d) T. Kim, S. J. McCarver, C. Lee and D. W. C. MacMillan, *Angew. Chem., Int. Ed.*, 2018, **57**, 3488–3492.

7 (a) E. R. Welin, C. Le, D. M. Arias-Rotondo, J. K. McCusker and D. W. C. MacMillan, *Science*, 2017, **355**, 380–384; (b) L. Yang, H. H. Lu, C. H. Lai, G. Li, W. Zhang, R. Cao, F. Y. Liu, C. Wang, J. L. Xiao and D. Xue, *Angew. Chem., Int. Ed.*, 2020, **59**, 12714–12719; (c) D. L. Zhu, H. X. Li, Z. M. Xu, H. Y. Li, D. J. Young and J. P. Lang, *Org. Chem. Front.*, 2019, **6**, 2353–2359.

8 (a) B. J. Shields, B. Kudisch, G. D. Scholes and A. G. Doyle, *J. Am. Chem. Soc.*, 2018, **140**, 3035–3039; (b) S. I. Ting, S. Garakyaraghi, C. M. Taliaferro, B. J. Shields, G. D. Scholes, F. N. Castellano and A. G. Doyle, *J. Am. Chem. Soc.*, 2020, **142**, 5800–5810; (c) L. Tian, N. A. Till, B. Kudisch, D. W. C. MacMillan and G. D. Scholes, *J. Am. Chem. Soc.*, 2020, **142**, 4555–4559; (d) P. C. Ma, S. H. Wang and H. Chen, *ACS Catal.*, 2020, **10**, 1–6; (e) D. A. Cagan,

G. D. Stroscio, A. Q. Cusumano and R. G. Hadt, *J. Phys. Chem. A*, 2020, **124**, 9915–9922.

9 (a) G. Wilke, *Angew. Chem., Int. Ed.*, 1988, **27**, 185–206; (b) J. Montgomery, *Acc. Chem. Res.*, 2000, **33**, 467–473; (c) T. Kurahashi and S. Matsubara, *Acc. Chem. Res.*, 2015, **48**, 1703–1716; (d) M. Ohashi, Y. Hoshimoto and S. Ogoshi, *Dalton Trans.*, 2015, **44**, 12060–12073.

10 (a) A. Nishimura, M. Ohashi and S. Ogoshi, *J. Am. Chem. Soc.*, 2012, **134**, 15692–15695; (b) H. Horie, T. Kurahashi and S. Matsubara, *Chem. Commun.*, 2012, **48**, 3866–3868; (c) S. Ogoshi, A. Nishimura and M. Ohashi, *Org. Lett.*, 2010, **12**, 3450–3452; (d) Y. K. Ni and J. Montgomery, *J. Am. Chem. Soc.*, 2004, **126**, 11162–11163; (e) T. Kawashima, M. Ohashi and S. Ogoshi, *J. Am. Chem. Soc.*, 2018, **140**, 17423–17427; (f) L. Liu and J. Montgomery, *J. Am. Chem. Soc.*, 2006, **128**, 5348–5349.

11 (a) S. Ogoshi, H. Ikeda and H. Kurosawa, *Angew. Chem., Int. Ed.*, 2007, **46**, 4930–4932; (b) Y. Kajita, S. Matsubara and T. Kurahashi, *J. Am. Chem. Soc.*, 2008, **130**, 6058–6059; (c) M. Ohashi, I. Takeda, M. Ikawa and S. Ogoshi, *J. Am. Chem. Soc.*, 2011, **133**, 18018–18021; (d) Y. Yoshida, T. Kurahashi and S. Matsubara, *Chem. Lett.*, 2011, **40**, 1140–1142; (e) T. Shiba, T. Kurahashi and S. Matsubara, *J. Am. Chem. Soc.*, 2013, **135**, 13636–13639; (f) Y. Hoshimoto, T. Ohata, M. Ohashi and S. Ogoshi, *Chem.–Eur. J.*, 2014, **20**, 4105–4110.

12 (a) Y. Kajita, T. Kurahashi and S. Matsubara, *J. Am. Chem. Soc.*, 2008, **130**, 17226–17227; (b) I. Koyama, T. Kurahashi and S. Matsubara, *J. Am. Chem. Soc.*, 2009, **131**, 1350–1351; (c) A. Ooguri, K. Nakai, T. Kurahashi and S. Matsubara, *J. Am. Chem. Soc.*, 2009, **131**, 13194–13195; (d) S. Sako, T. Kurahashi and S. Matsubara, *Chem. Commun.*, 2011, **47**, 6150–6152.

13 (a) T. Inami, Y. Baba, T. Kurahashi and S. Matsubara, *Org. Lett.*, 2011, **13**, 1912–1915; (b) T. Inami, T. Takahashi, T. Kurahashi and S. Matsubara, *J. Am. Chem. Soc.*, 2019, **141**, 12541–12544.

14 L. Adak, W. C. Chan and N. Yoshikai, *Chem.–Asian J.*, 2011, **6**, 359–362.

15 M. Kasha, *Discuss. Faraday Soc.*, 1950, **9**, 14–19.

16 A. B. P. Lever, *Inorganic Electronic Spectroscopy*, Elsevier, 1984.

17 A. Basu, H. D. Gafney and T. C. Strekas, *Inorg. Chem.*, 1982, **21**, 2231–2235.

18 (a) O. A. Vydrov and G. E. Scuseria, *J. Chem. Phys.*, 2006, **125**, 234109; (b) O. A. Vydrov, J. Heyd, A. V. Krukau and G. E. Scuseria, *J. Chem. Phys.*, 2006, **125**, 074106; (c) S. Ragot and P. J. Becker, *J. Chem. Phys.*, 2006, **125**, 154109.

19 (a) M. M. Francl, W. J. Pietro, W. J. Hehre, J. S. Binkley, M. S. Gordon, D. J. Defrees and J. A. Pople, *J. Chem. Phys.*, 1982, **77**, 3654–3665; (b) R. Krishnan, J. S. Binkley, R. Seeger and J. A. Pople, *J. Chem. Phys.*, 1980, **72**, 650–654; (c) A. D. McLean and G. S. Chandler, *J. Chem. Phys.*, 1980, **72**, 5639–5648.

20 J. Shin, S. Gwon, S. Kim, J. Lee and K. Park, *J. Am. Chem. Soc.*, 2020, **142**, 4173–4183.

21 R. Fayad, S. Engl, E. O. Danilov, C. E. Hauke, O. Reiser and F. N. Castellano, *J. Phys. Chem. Lett.*, 2020, **11**, 5345–5349.

22 (*a*) D. A. Prinslow and V. Vaida, *J. Am. Chem. Soc.*, 1987, **109**, 5097–5100; (*b*) A. Rosa, G. Ricciardi, E. J. Baerends and D. J. Stufkens, *Inorg. Chem.*, 1996, **35**, 2886–2897; (*c*) C. Daniel, *Coord. Chem. Rev.*, 2003, **238**, 143–166.